Mantle Phase Change Detection from Stochastic Tomography

Vernon F. Cormier[1], Yiteng Tian[1], and Yingcai Zheng[2]

[1]Department of Physics, University of Connecticut

[2]Department of Earth and Atmospheric Sciences, University of Houston

Corresponding author: Vernon Cormier (vernon.cormier@uconn.edu)

†Vernon F. Cormier, Department of Physics, University of Connecticut, 196A Auditorium Road, Storrs, CT 06269-3046

Index terms: 7203, 7208, 7260, 3611, 3612

Key Points:

- An application of stochastic tomography exhibits peaks in depth in the inverted heterogeneity spectrum of the upper mantle.
- These peaks correlate with the majority of predicted mineral phase changes in the mantle.
- Phase change detection requires a dense seismic array and distributions of groups of earthquakes and estimates of their mechanisms.

Abstract

Peaks are observed in a depth dependent power spectrum of P-wave velocity fluctuations determined from an inversion of P wave coherences observed by the USArray. These peaks correlate with the depths of the majority of silicate mineral phase changes predicted by a thermodynamic model of the upper 1000 km of a pyrolitic mantle. To within ± 25 km we identify the phase change of orthopyroxene to HP-clinopyroxene at 275 km, the olivine to wadsleyite phase change at 425 km, the wadlsleyite to ringwoodite phase change at 505 km, and the initiation of an akimotoite phase at 600 km and a signature of a phase change at 775 km, both associated with the existence of fragments of subducted oceanic crust. Non-detection of a phase change at or near 660 is consistent with the phase change of ringwoodite to Mg-perovskite and magnesiowusite occurring over a depth interval much smaller than 25 km.

Plain Language Summary

Fluctuations in amplitude and traveltimes of seismic P waves from deep earthquakes observed at the USArray of seismic stations are inverted for a depth dependent spectrum of the intensity P wave velocity fluctuations. Peaks with depth of this spectrum correlate with the depths predicted for changes in the arrangements of atoms of the silicate minerals comprising the upper 1000 km of Earth's mantle.

1 Introduction

Modern reference Earth models typically have few first order discontinuities in the upper mantle. These include commonly agreed ones at or near 400 and 660 km depth, which are interpreted to be changes in solid phase of silicate minerals from the effect of increasing pressure with depth. They are routinely observed in complex, double-triplicated, body waveforms between 15^{o} to 35^{o}, associated with near grazing incidence on two nearly discontinuous increases in P and S wave velocities and densities at these depths. They are often also observed from partial reflections at steeper angles of incidence from P to S conversions in receiver functions and in underside reflections and conversions arriving as precursors to PP waves. In each of these observations the detection of the sharp change in velocity and density depends on the width of the phase transition in depth being narrower than the characteristic wavelength of the incident body wave. Dziewonski & Anderson (1981) recognized early that the steep velocity gradients required to

exist in the mantle transition zone between the 400 and 660 discontinuities in PREM likely masked a more complex set of mineral phase transitions occurring over broader intervals in depth. In addition to those in the transition zone, the existences of other phase changes may manifest themselves not as reflective discontinuities but rather as broader zones of increased small-scale heterogeneity.

Small-scale heterogeneities, unresolvable by conventional tomography, have detectible signatures in the fluctuation of amplitudes and travel times observed across seismic arrays. Numerical simulations have shown that small-scale heterogeneity in the upper mantle can affect the wavefront of an incident teleseismic wave beneath an array. Small differences in the angle of approach of wavefronts, on the order of a several degrees or less, can produce unique signatures in amplitude and phase fluctuations due to differences in the sensitivity of the wavefronts to the small-scale structure (e.g., Zheng & Wu 2008; Tkalcic et al., 2010). Measurement of these fluctuations between array elements can be exploited to invert for the spectrum of heterogeneity beneath the array with techniques that have been named stochastic tomography (Wu & Flatté, 1990; Wu & Xie, 1991, Zheng & Wu, 2008).

Applying stochastic tomography to amplitude and phase fluctuations observed from three groups of deep focus earthquakes by elements of the USArray, we inverted for a depth dependent heterogeneity spectrum in the upper 1000 km beneath the western US (Cormier et al., 2020). The inverted heterogeneity spectrum is characterized by a series of peaks that strongly correlate with the depths of silicate phase changes predicted by thermodynamic models (Stixrude & Lithgow-Bertelloni, 2007, 2012). The majority of these detected phase changes are expressed by relatively weak changes in seismic velocity gradient spaced over a depth range on the order of or larger than a wavelength, making them undetectable by high frequency, reflected and converted, body waves.

In this paper, we interpret in detail the individual peaks in the heterogeneity spectrum we published in a smoothed form, showing them in a raw, depth-discretized, form with error bars. From these interpretations we estimate constraints on the depth and widths of the detected phase

transitions. We first briefly review the application of stochastic tomography in our previous paper (hereafter referred to as CICP 2020). We conclude with a commentary on the experimental design needed to resolve peaks in the heterogeneity spectrum with depth. In conjunction with this paper we also provide downloadable Python and Matlab scripts to assist researchers in designing experiments with stochastic tomography (Tian and Cormier, 2020). These example scripts treat the effects of earthquake moment tensors and source-time functions on the reference wavefields defining coherence measurements.

2 Methods and Application

Transmission fluctuation coherence measurements (eqs. 1a-d) are the starting point for stochastic tomography. We consider the recorded fields due to two plane waves, PW1 and PW2. We use $U_1(x_1)$ for the recorded field at x_1 for PW1. Likewise, we use $U_2(x_2)$ for the recorded field at x_2 for PW2. Both fields propagate through the same heterogeneous medium. We also consider their corresponding reference fields (no heterogeneities), $U_{1ref}(x_1)$ and $U_{2ref}(x_2)$, respectively. We can write the seismic fields in amplitude and phase terms, for example, $U_1 = u_1 \exp[i\omega t] = u_1 \exp[i\phi]$ and $U_{1ref} = u_{1ref} \exp[i\omega t_{ref}] = u_{1ref} \exp[i\phi_{ref}]$. Similar representations are applied to PW2. A Rytov approximation provides the relationship between the scattered field and the reference field: $U_1 = U_{1ref} e^{\Psi_1}$. The complex function Ψ has a real part, which is the logarithmic amplitude, and an imaginary part, which is the phase (or traveltime) difference. In our work, the observables are the ratios of log amplitude and travel time differences (eqs. 1c-d) from those computed in a reference Earth model. Transverse coherence functions are constructed as a function of the lag distance x between pairs of receivers. The brace brackets in eqs. 1a-b, define the logarithmic amplitude $\langle u_1 u_2 \rangle$ and $\langle \phi_1 \phi_2 \rangle$ phase coherences by averaging measurements for a specific lag distance over all combinations of two receivers in an array separated by that lag distance. Non-dimensional coherence values range from zero (no correlation in signal amplitude and traveltime fluctuations) at neighboring receivers to 1 for perfect correlation.

$$(1a) \qquad \langle u_1 u_2 \rangle = \frac{1}{2}\mathrm{Re}\langle \psi_1 \psi_2^* \rangle + \frac{1}{2}\mathrm{Re}\langle \psi_1 \psi_2 \rangle$$

$$(1b) \qquad \langle \phi_1 \phi_2 \rangle = \frac{1}{2}\mathrm{Re}\langle \psi_1 \psi_2^* \rangle - \frac{1}{2}\mathrm{Re}\langle \psi_1 \psi_2 \rangle, \qquad \textit{where}$$

$$(1c) \qquad \hat{\psi}(\omega) = \ln(u / u_{ref}) + i\omega(t - t_{ref})$$

$$(1d) \qquad u = \frac{\psi + \psi^*}{2} \quad \textit{and} \quad \phi = \frac{\psi - \psi^*}{2}$$

To construct the complex functions $\hat{\psi}(\omega)$, we measure u and u_{ref} from observed and synthetic seismograms around the direct P waves from the outputs of a multi-taper filter at 0.7 Hz, and measure the traveltime difference $t - t_{ref}$ from cross-correlation of observed and predicted reference waveforms.

Stochastic tomography assumes that the functional behaviors of the coherences with lag distance are due to the interference of plane waves scattered by heterogeneity having an unknown power spectrum as a function of wavenumber and depth. The transverse coherences can be written as an integral over horizontal wavenumber and depth, with an integrand containing the power spectrum (eqs. 2a-c).

$$(2a) \quad \langle u_1 u_2 \rangle = (2\pi)^{-1} \int_0^H d\xi a_1(\xi) a_2(\xi) \int_0^\infty J_0\left[(\kappa R(\xi)\right] \sin\left[\omega\theta_1(\xi)\right] \sin\left[\omega\theta_2(\xi)\right] P(\xi,\kappa)\kappa d\kappa$$

$$(2b) \quad \langle \phi_1 \phi_2 \rangle = (2\pi)^{-1} \int_0^H d\xi a_1(\xi) a_2(\xi) \int_0^\infty J_0\left[(\kappa R(\xi)\right] \cos\left[\omega\theta_1(\xi)\right] \cos\left[\omega\theta_2(\xi)\right] P(\xi,\kappa)\kappa d\kappa$$

$$(2c) \quad \langle u_1 \phi_2 \rangle = (2\pi)^{-1} \int_0^H d\xi a_1(\xi) a_2(\xi) \int_0^\infty J_0\left[(\kappa R(\xi)\right] \sin\left[\omega\theta_1(\xi)\right] \cos\left[\omega\theta_2(\xi)\right] P(\xi,\kappa)\kappa d\kappa$$

In eqs. 2a-c, P is the power spectrum as a function of depth ξ and horizontal wavenumber κ. H is the thickness of a heterogeneous layer. Functions a_1, a_2, θ_1, and θ_2 are defined in CICP 2020. The function R appearing in the argument of the Bessel function J_0 is the horizontal distance between the pair of rays arriving at a specific lag distance at depth ξ. The average sum of a coherence measurement at each lag from many sources at different distances and azimuths

128 can, in principle, be sensitive to the effects of scatterers whose size may be less than the spacing
129 of array elements.
130
131 These integrals can be discretized and set-up as a linearized inverse problem in which the
132 squared difference of the observed coherences and predicted coherences of an unknown power
133 spectrum are minimized. The discretized forms of eqs.2a-c and the object function to be
134 minimized are given in Appendix B of CICP 2020.
135
136 In CICP 2020 the coherence data we chose to invert were 3 groups of deep focus earthquakes
137 (Marianas, Tonga-Kermedec, and South America) observed by elements of the US array and
138 transportable array in the western US (Fig. 1). Deep focus events were chosen to avoid the
139 effects of heterogeneity concentrated in the upper mantle near the source and to eliminate the
140 effects of near source reflections. P waveforms of 21,205 deep focus earthquakes having moment
141 magnitudes Mw between 5.8 to 6.2 were downloaded from the Data Management Center of
142 IRIS. About 40% of these had sufficiently high signal to noise ratios and simple apparent
143 source-time functions to include in the coherence measurements. Within each earthquake group,
144 measured coherences are averaged at all receiver pairs corresponding to a specific lag.
145 Wavefront healing due to propagation from the source to the teleseismic receivers as well as
146 coherence over earthquakes aids in eliminating any source-side heterogeneity effects. A joint
147 inversion of data comprising 3 wavefronts arriving from widely different azimuths, whose rays
148 cross at variable depths beneath the array, makes it possible to achieve a sensitivity to
149 heterogeneity scales slightly smaller than the spacing of array elements.

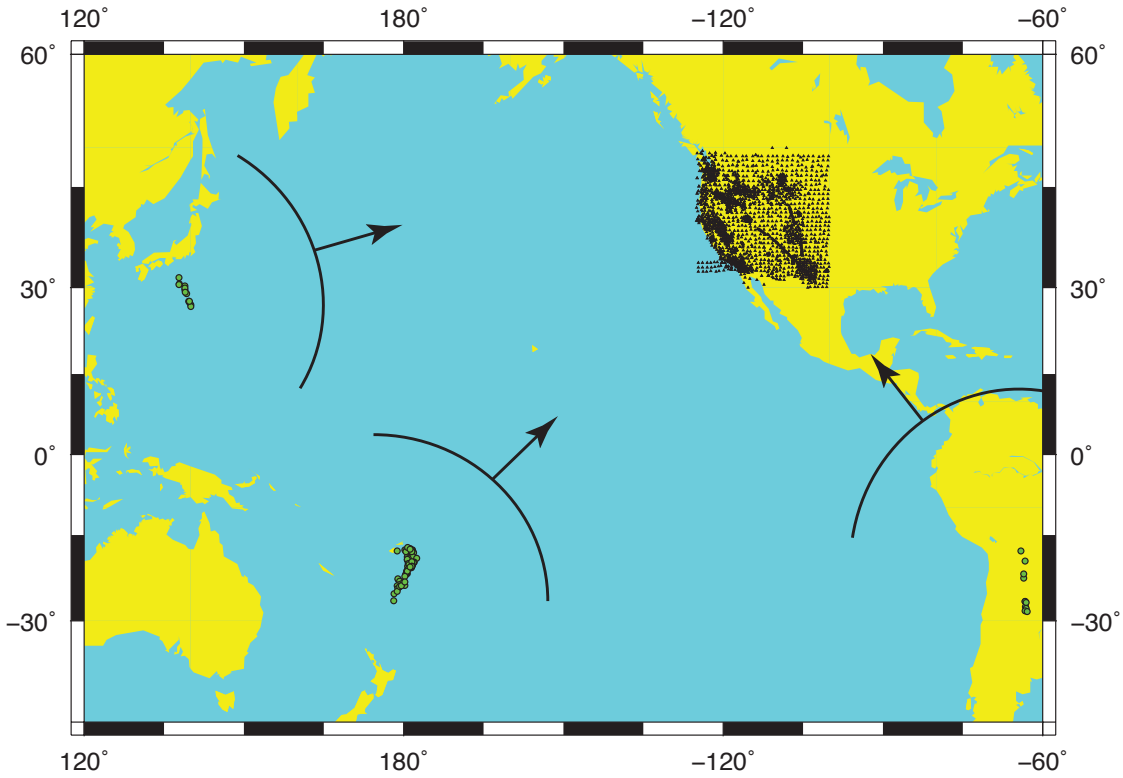

Figure 1. Hypocenters of three deep-focus earthquake groups and US Array seismic stations used in the inversion of P wave coherence for the upper mantle heterogeneity spectrum.

The inclusion of the effects of the specific earthquake source-time functions and radiation patterns in u_{ref} are essential to isolating the effects of forward scattering from those of the source. To achieve this for each event the reference synthetic seismogram u_{ref} at each array element was computed from the IRIS Syngine service (Nissen-Meyer, et al., 2014; https://service.iris.edu/irisws/syngine) in the AK135-F Earth model (Montagner & Kennett, 1995) using the known moment tensor solution for each event from the GCMT service (Ekstrom et al., 2012; https://www.globalcmt.org) and an empirical source time function determined by stacking P waves from each event in the 40^o to 90^o distance range.

We first inverted for a constant heterogeneity spectrum with depth in which the shape of the power spectrum was defined by 4 parameters. We then assumed that the spectral shape in wavenumber determined from the single layer inversion was constant in depth but allowed its peak power to vary with depth in 40, 25 km thick, layers. Comparing the depth dependent inversion to the single layer inversion, the squared coefficient of determination increased from 0.74 to 0.80 and the reduced χ^2 decreased from 1.65 to 1.05. The significantly smaller, but not less than 1, χ^2 for the depth dependent spectrum is consistent with an improved fit, but not an over- fit due to the assumption of a larger number of unknown parameters. Plots of our observed and predicted coherences from both types of inversions are shown in CICP 2020.

3 Results

3.1 Interpretation of the depth dependent heterogeneity spectrum

Results of our inversion for a depth dependent heterogeneity spectrum for the upper 1000 km of the mantle beneath the western US for the root-mean-square (rms) P velocity fluctuations are shown in Fig. 2. The complexity of the spectrum with depth, consisting of narrow peaks, does not resemble a smooth 1-D depth spectrum, with power decaying with depth in the upper mantle, commonly resolved in conventional travel time tomography. The error bars in depth in Fig. 2 are fixed at 25 km to equal the sampling rate for the 40 depth values used in our inversion. The ordinate error bars in the power of rms velocity fluctuation are taken to be 10% of the ordinate value. To our surprise the depth of the peaks correlate well with ones that have been predicted in a thermodynamic model of mantle heterogeneity by Stixrude & Lithgow-Bertelloni (2007). This model assumes a pyrolitic composition in which chemistry and phase vary with depth to achieve an equilibrium state that minimizes Gibbs free energy. The effective temperature derivative of shear velocity for this model shown in Fig. 2 assumes an adiabatic temperature gradient and a 1600^{o} K potential temperature. In related models, Stixrude & Lithgow-Bertelloni (2012) demonstrate the effects of varying potential temperature and mechanical mixing of harzburgite and basalt to simulate the effects of slab cycling.

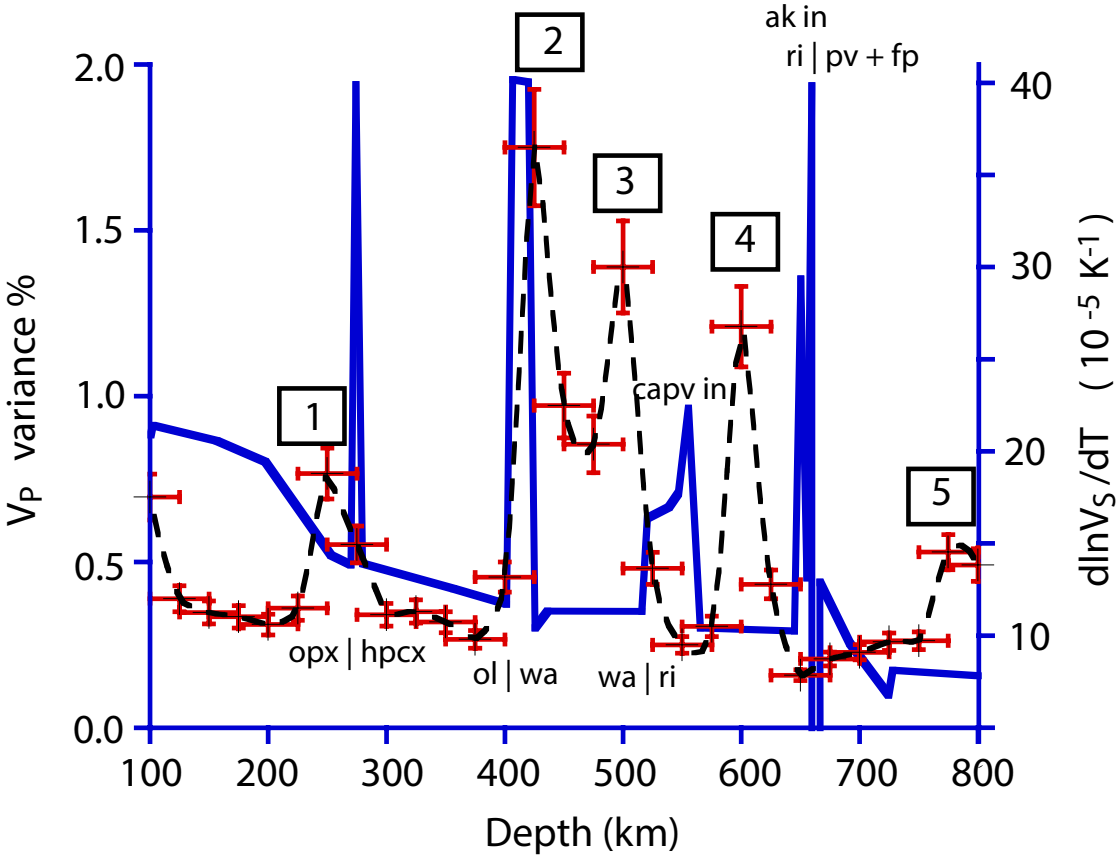

Figure 2. The depth dependent heterogeneity spectrum for the rms fluctuation of P wave velocity in the upper 1000 km of the mantle compared with the temperature derivative of shear velocity predicted in the thermodynamic pyrolitic model in Stixrude & Lithgow-Bertelloni (2007). Numbered silicate mineral phase changes next to peaks in the temperature derivative are keyed to interpretations in this section.

Predicted peaks in the temperature derivative of seismic velocities are from metamorphic contributions due to phase and chemistry changes (Fig. 3). The expression of these changes in seismic velocity can either be sharp or spread out over a depth range bounded by two changes in the gradient of seismic velocity. If sharp, the phase change can be detectable from reflected, converted, or multipathed body waves, and the effect of lateral temperature variations will be expressed as topography on an apparent seismic reflector. If spread out over a depth range, the phase change will not be detectable in seismic reflections or receiver function processing, but will be detectable as discrete scatterers in a narrow range of depth. In this case, the horizontal

length scale of the scatterers will be related to the lateral scale of temperature variations and the vertical scale to the width of the depth (pressure) range over which the phase change occurs. It is just this type of phase change that can be detectable by stochastic tomography, which seeks to image stochastically described forward scattering with depth. Note in Fig.3 that the depth sampling of estimated scattering power may not be able to detect phase changes that occur over a depth interval shorter than the sampling rate.

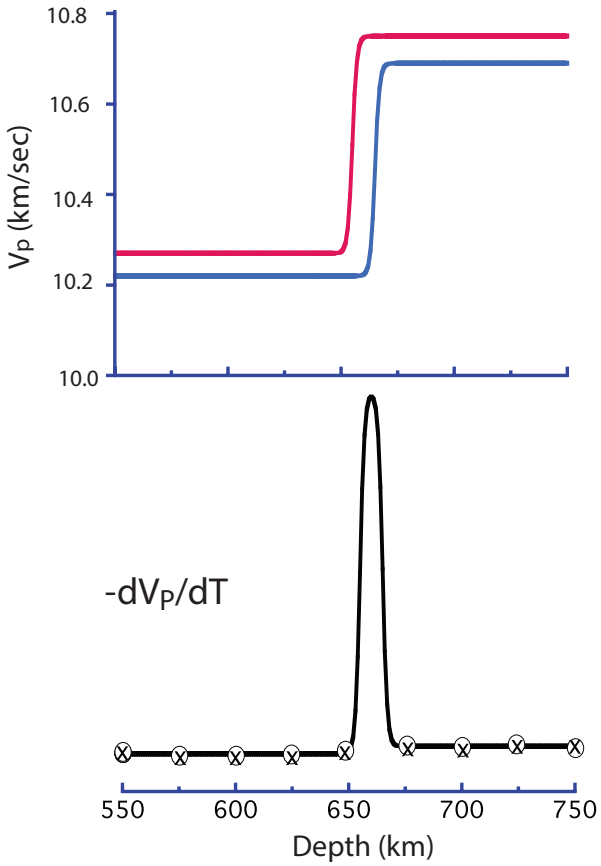

Figure 3. Top: the effect of a temperature variation on the P velocity due to an endothermic phase change near 660 km depth (red hotter/blue colder) Bottom: the metamorphic contribution to the temperature derivative of P velocity computed by a difference derivative. Crosses are at

220 the 25 km depth-sampling interval of the heterogeneity spectrum derived from the stochastic
221 tomography inversion.
222
223 Keeping these factors and limitations in mind, we can begin to interpret the correlations in Fig. 2
224 between the predicted peaks in the temperature derivative of seismic velocity from the
225 thermodynamic mantle model and the peaks in depth of the heterogeneity power determined
226 from stochastic tomography. A possible interpretation of the correlations follows:
227
228 (1) A peak at 250 ±25 km correlates with a predicted phase change of orthopyroxene to HP-
229 clinopyroxene at 275 km.
230 (2) A peak at 425 ±25 km correlates with a predicted phase change of olivine to wadsleyite
231 between 405 to 418 km.
232 (3) A peak at 500 ±25 km correlates with a predicted phase change of wadsleyite to
233 ringwoodite at 505 km. The predicted signal in the temperature derivative of velocity,
234 however, consists of a relatively wide peak in which the shallower wadsleyite to
235 ringwoodite phase change interferes with an initiation of a deeper calcium perovskite
236 phase (capv in) at 545 km.
237 (4) A peak at 600 ±25 km nearly correlates with two predicted interfering phase changes: an
238 exothermic phase change with the initiation of akimotoite (ak in) having a positive
239 temperature derivative of velocity, followed by predicted endothermic phase change from
240 ringwoodite to perovskite and ferropericlase (ri to pv + fp). In the thermodynamic model
241 these two interfering phase changes occur between 650 to 660 km depth.
242 (5) A peak at 775 ±25 km correlates with one predicted at 785 km in mechanical mixtures of
243 basalt and harzburgite having a basalt fraction of 18%, indicative of a phase change in
244 subducted oceanic crust.
245
246 The differences between detected and predicted phase changes will depend on the accuracy of
247 the assumptions in the thermodynamic model and the sampling and errors in the power spectrum
248 of heterogeneity determined from stochastic tomography. The depth accuracy of the
249 thermodynamic model depends on the validity of the assumed petrologic model and the physical
250 properties of minerals determined from combinations of experimental observations and ab initio

calculations. The depth accuracy of the power spectrum largely depends on the depth-sampling rate that can be resolved in the inversion of coherences, which depends on sensor spacing and its geometry and the azimuthal and depth distribution of seismic events.

For the 25 km depth sampling possible in this study, some general conclusions can be made about the achievable accuracy for stochastic tomography applied to the US Array. Except for a disagreement between an observed and predicted 660 km seismic discontinuity, the depths of the majority of predicted and observed phase changes agree within estimated errors. This suggests that a pyrolitic theromodynamic model having a 1600^{o} potential temperature and some mechanical mixing of subducted basalt is an adequate model for the upper 1000 km beneath the western US. The depth of nearly all other predicted phase changes has been detected within estimated error of +- 25 km, suggesting that the transition width of at least some of these phase changes may equal or exceed 25 km.

The disagreement between the detected (600 km) and predicted (660 km), last and deepest, major phase change is too large to be explained by a plausible hotter mantle temperature in this broad region. A global 660 km discontinuity has been largely confirmed in many seismic studies and is generally the most robustly detected discontinuity even by reflected body waves having dominant frequencies approaching 1 Hz (e.g., Deuss et al., 2006). Its signature in receiver functions (Andrews & Deuss, 2006), however, can be complex, in agreement with the complex phase changes predicted from thermodynamic models at and near this depth (Xu et al., 2008). A partial explanation for a positive detection at 600 km but not 660 km is that the 25 km sampling rate in the inversion is simply too coarse to resolve the complex signal of two closely spaced phase changes. In addition, the positive detection at 600 km may instead be a detection of the predicted transformation of high-pressure clinopyroxene to akimotoite initiating closer to 600 rather than 650 km (Hao et al., 2019), having a transition width in depth on the order of 25 km or greater. The predicted phase change at 660 km of ringwoodite to Mg-perovskite and magnesiowusite, estimated to have a transition width of 2 km (Ishii et al, 2019), may be more easily detectable from reflected and converted body waves than from a stochastic power spectrum having a sampling interval of 25 km.

The detection of an akimototite transition at 600 km, indicative of the existence of regions of colder mantle temperatures (Hogrefe et al., 1994), coupled with a phase transition at 775 km, is consistent with the history of the subduction of the Farallon plate beneath the western US. Tomographic images of the shear velocity structure of the mantle beneath this region reveal evidence of both slab stagnation and fragmentation in the lower mantle transition zone as well as penetration beneath 660 km (Schmid et al., 2002).

3.2 Comparison with non-depth dependent heterogeneity spectra

It is useful to factor out the wavenumber dependence from our depth dependent spectrum and compare its spectrum against other non-depth dependent, stochastic models of upper mantle heterogeneity. In the context of understanding how lateral temperature differences drive mantle heterogeneity such a comparison can provide some constraints on the compositional and temperature variations in the upper mantle at scale lengths intermediate between those estimated from global travel-time tomography and the coda of high-frequency body waves.

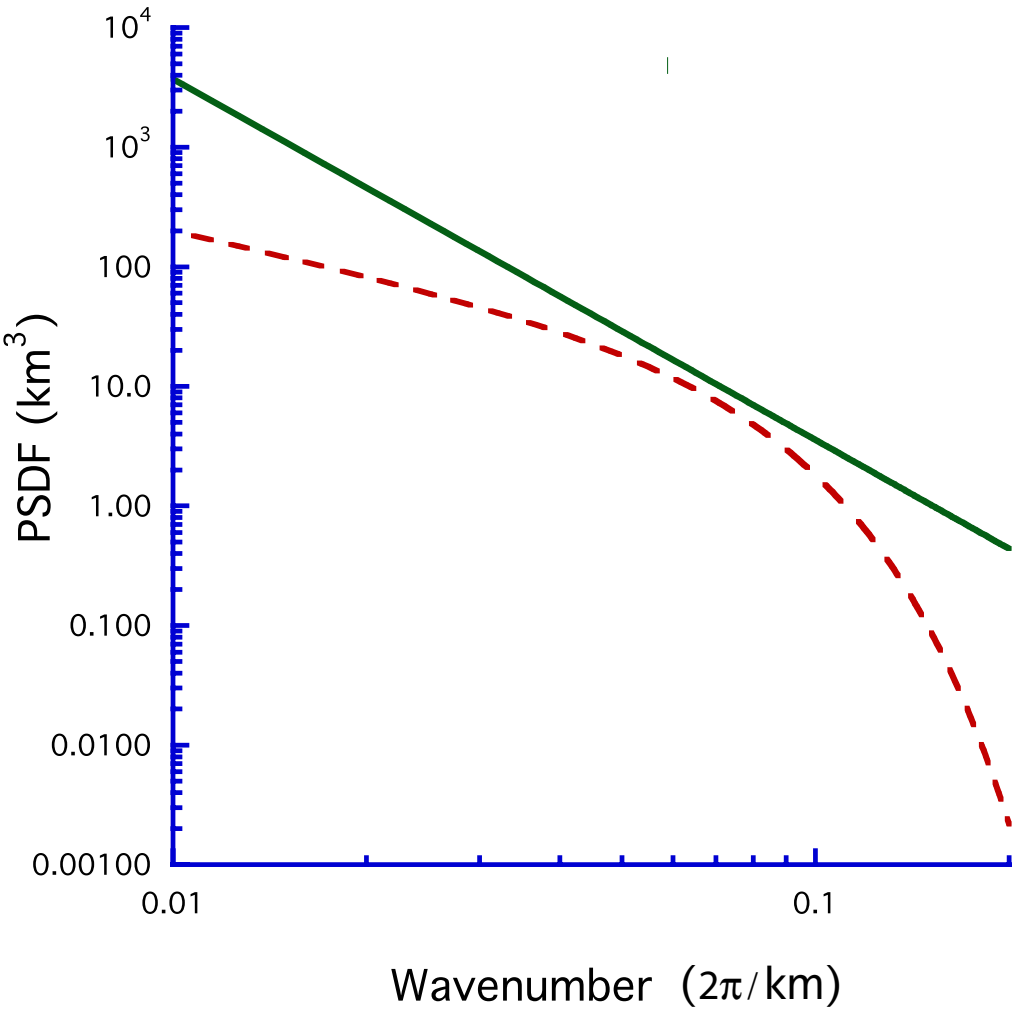

296

297 **Figure 4.** Mancinelli et al's (2016) heterogeneity spectrum (solid green line) compared with our
298 single layer (dashed red line), isotropic heterogeneity spectrum.

299

300 Mancinelli et al. estimated a 1-D von Karman spectrum for the upper mantle based on the
301 scattered coda of broadband body waves and the power spectrum of larger scale heterogeneity
302 resolved by global tomography. Our inverted heterogeneity spectrum was a 3-D isotropic
303 spectrum. Hence, to make the comparison shown in Fig. 4, we converted the 1-D spectrum in
304 Mancinelli et al. to a 3-D isotropic spectrum for a von Karman medium using formulas in Sato et
305 al. (2012). Our spectrum was parameterized by shape parameters recommended by Klimes
306 (2002), consisting of a product of a low pass and high pass filter in wavenumber. We chose this
307 type of parameterization to recognize that the sensitivity of our coherence data peaked around a
308 narrow band in wavenumber. In contrast, the data fit by Mancinelli et al. weight the effects of

heterogeneity over a much broader band of wavenumber, corresponding to frequencies from millihertz to 10 Hz. The two spectra nearly coincide in a narrow wavenumber band centered near 0.065 km^{-1}. From the region of match in wavenumber, we conclude that scale length of heterogeneities induced by lateral variations in upper mantle phase transitions has a lateral scale length on the order of 100 km. This suggests that our coherence measurements reveal the existence of a significant lateral scale on the order of 100 km for variations in chemistry, temperature (100^o to 500^o K), or both.

4 Conclusions

The application of stochastic tomography to invert for a depth dependent heterogeneity spectrum in the upper 1000 km of the mantle reveals a strong correlation with the majority of predicted phase changes from a thermodynamic model of a pyrolitic mantle. This demonstrates that stochastic tomography has the potential to detect mantle phase changes that do not exhibit changes in seismic velocity and density over short depth intervals. These types of phase changes are characterized by paired changes in velocity gradient over a transition depth that may be equal to or larger than the wavelength of a body wave.

Results from a depth-sampling interval of 25 km for the inverted spectrum for the upper mantle beneath western North America suggest that many of these phase changes may occur over a range in depth equal to or greater than 25 km. An exception is our non-detection of the phase transition at 660 km, consistent with a transition interval in depth that may be as small as 2 km (0.1 GPa).

To detect changes in mantle phases with stochastic tomography requires not only a depth-sampling interval on the order of 25 km or less, but also estimation of the amplitude and phase effects of source radiation patterns and source-time functions. Resolution will also be improved by averaging of measured coherences at each lag over a large number of earthquakes arriving from sufficiently different azimuths. The 40 km spacing of the US Array elements and the availability of waveforms from 3 widely separated groups of deep focus earthquakes, having simple source-time functions, makes this possible for at least the western US. Similar to the 1970's discovery of the 400 and 660 km mantle velocity discontinuities (Burdick & Helmberger,

1978), which required the incorporation of the effects of earthquake sources, the detection of less pronounced mantle phase changes, will generally require routine source-time function and moment tensor estimation.

Acknowledgments and Data

This study was supported by the National Science Foundation under grant EAR 14-46509 (Vernon Cormier and Yiteng Tian) and grant EAR 16-21878 (Yingcai Zheng). Interpretations benefited from discussions with Lars Stixrude, Carolina Lithgow-Bertelloni, and Hao Hu. Figure 1 was drawn using the Generic Mapping Tools (Wessel and Smith, 1998).

Waveform data and services for centroid moment tensors and synthetic seismograms are available from the Incorporated Research Institutions for Seismology through the web site https://www.iris.edu. Matlab and Python scripts for processing and inverting amplitude and phase coherences for single layer and depth dependent heterogeneity spectra are available for download from the sites in the Tian & Cormier (2020) entry in the References.

References

Andrews, J., and Deuss, A. (2008), Detailed nature of the 660 km region of the mantle from global receiver function data. *J. Geophys. Res.*, 113 (B6). doi:10.1029/2007JB005111.

Burdick, L.J., and Helmberger, D.V. (1978), The upper mantle P velocity structure of the western United States. *J. Geophys. Res.*, 83 (B4), 1699-1712.

Cormier, V.F., Tian, Y., & Zheng, Y. (2020), Heterogeneity spectrum of Earth's upper mantle obtained from the coherence of teleseismic P waves. *Commun. Comp. Phys.*, 28, 74-97. doi: 10.4208/cicp.OA-2018-0079.

Deuss., A., Redfern, S.A.T., Chambers, K., & Woodhouse, J.H. (2006), The nature of the 660 km discontinuity in Earth's mantle from global seismic observations of PP precursors. *Science*, 311, 198-201.

Dziewonski, A.M., & Anderson, D.L., (1981), Preliminary Reference Earth Model. Phys. Earth Planet. Int., 25 (4), 297-356.

Ekstrom, G., Nettles, M., & Dziewoski, A. M., (2012), The global CMT project 2004-2010: Centroid moment tensors for 13,017 earthquakes. *Phys. Earth Planet. Int.,* 200-201, 1-9, doi: 10.1016/j.pepi.2012.04.002.

Hao, S., Wang, W., Qian, W., & Wu, Z. (2019), Elasticity of akimotoite under the mantle conditions: Implications for multiple discontinuities and seismic anisotropies at the depth ~600-750 km in subduction zones. *Earth Planet. Sci. Lett.,* 528, 115830.

Hogrefe, A., Rubie, D.C., Sharp, T.G., (1994), Metastability of enstatite in deep subducting lithosphere. *Nature*, 372 351-353.

Ishii, T., Huang, T., Myhill, R., Fei, H. Koemets, L., Liu, Z., Maeda, F., Yuan, L., Wang, L., Druzhbin, D., Yamamoto, T., Bhat, S., Faria, R., Kawazoe, T., Tsujino, N., Kulik, E., Higo, Y, Tange, Y., & Katsura, T. (2019), Sharp 660-km discontinuity controlled by extremely narrow binary post-spinel transition. *Nature Geoscience*, 12, 869-872.

Klimes, K. (2002), Correlation functions of random media. *Pure Appl. Geophys.*, 159 1811-1831.

Mancinelli, N., and Shearer, P., Liu, Q. (2016), Constraints on the heterogeneity spectrum of Earth's upper mantle. *J. Geophys. Res.,* 121 (5), 3703-3721.

Montagner, J.P., and Kennett, B.L.N., (1995), How to reconcile body-wave and normal-mode reference Earth models? *Geophys. J. Int.*, 135-229-248.

Nissen-Meyer, T., van Driel, M., Stähler, S. C., Hosseini, K., Hempel, S., Auer, L., Colombi, A., & Fournier, A. (2014) AxiSEM: broadband 3-D seismic wavefields in axisymmetric media.

Solid Earth, 5, 425-445, https://doi.org/10.5194/se-5-425-2014.

Sato, H., Fehler, M.C., & Maeda, T. (2012), *Seismic Wave Propagation and Scattering in the Heterogeneous Earth,* 2nd edn., Springer-Verlag.

Schmid, C., Goes, S., van der Lee, S., & Giardini, D. (2002), Fate of the Cenozoic Farallon slab from comparison of kinematic thermal modeling with tomographic images. *Earth and Planet. Sci. Lett.,* 204, 17-32.

Stixrude, R., & Lithgow-Bertelloni, C. (2007), Influence of phase transformations on lateral dynamics in Earth's mantle. *Earth Planet. Sci. Lett,* 263, 45-55.

Stixrude, R., & Lithgow-Bertelloni, C. (2012), Geophysics of chemical heterogeneity in the mantle. *Ann. Rev. Earth Planet. Sci*., 40, 569-595.

Tian, Y., & Cormier, V.F., (2020), https://github.com/vernoncormier/stochastic_tomography, doi:/10.528/zenodo.4000538.

Tkalčić, H., Cormier, V.F., Kennett,B.L.N., & He, K. (2010), Steep reflections from the Earth's core reveal small-scale heterogeneity in the upper mantle. *Phys. Earth Planet. Int.*, 178, 80-91. doi: 10.1016/j.pepi.2009.08.004.

Wessel, P., and Smith, W.H.F. (1998), New, improved version of the Generic Mapping Tools released, *Eos Trans. AGU*, 79, 579.

Wu, R.S., & Flatté, S. (1990), Transmission fluctuations across an array and heterogeneities in the crust and upper mantle. *Pure Appl. Geophys.*, 132, 175-196.

Wu, R.S., & Xie, X. (1991), Numerical tests of stochastic tomography. *Phys. Earth Planet. Inter.*, 67 (1991) 180-193.

Xu, W., Lithgow-Bertelloni, C., Stixurde, L., and Ritsema, J. (2008), The effect of bulk composition and temperature on mantle seismic structure. *Earth. Planet. Sci. Lett.*, 275, 70-79.

Zheng, Y.,Wu, R.-S., (2008), Theory of transmission fluctuations in random media with a depth dependent background velocity structure. *Adv. Geophys.*, 50, 21-41.